Electronic Supplementary Information

Multifaceted [36]octaphyrin (1.1.1.1.1.1.1.1) :

Deprotonation-induced switching among nonaromatic, Möbius aromatic and Hückel antiaromatic species

Won-Young Cha,[a] Takanori Soya,[b] Takayuki Tanaka,[b] Hirotaka Mori,[b] Yongseok Hong,[a] Sangsu Lee,[a] Kyu Hyung Park,[a] Atsuhiro Osuka*,[b] and Dongho Kim*,[a]

[a]Department of Chemistry, Yonsei University, Seoul 120-749, Korea.

[b]Department of Chemistry, Graduate School of Science, Kyoto University, Sakyo-ku, Kyoto, 606-8502, Japan.

E-mail: dongho@yonsei.ac.kr, osuka@kuchem.kyoto-u.ac.jp

Contents

1. Instrumentations and materials.

All reagents and solvents were of commercial reagent grade and were used without further purification. ^{1}H and ^{13}C NMR spectra were recorded on a JEOL ECA-600 spectrometer, and chemical shifts were reported as the δ scale in ppm relative to the internal standards $CHCl_3$ (δ = 7.26 ppm for ^{1}H). Hexafluorobenzene (δ = –162.9 ppm) was used as external standard for ^{19}F NMR measurements. X-Ray crystallographic data was obtained by using a Rigaku XtaLAB P-200 system. The structures were solved by using direct methods (SHELX-97 or SIR-97). Structure refinements were carried out by using SHELXL-98. Steady-state absorption spectra were obtained with an UV-VIS-NIR spectrometer (Varian, Cary5000) and steady-state fluorescence spectra were measured on a Hitachi model F-2500 fluorescence spectrophotometer and a Scinco model FS-2. The femtosecond time-resolved transient absorption (fs-TA) spectrometer consists of an optical parametric amplifier (OPA; Palitra, Quantronix) pumped by a Ti:sapphire regenerative amplifier system (Integra-C, Quantronix) operating at 1 kHz repetition rate and an optical detection system. The generated OPA pulses have a pulse width of ~ 100 fs and an average power of 1 mW in the range of 280-2700 nm, which are used as pump pulses. White light continuum (WLC) probe pulses were generated using a sapphire window (3 mm thick) by focusing a small portion of the fundamental 800 nm pulses which was picked off by a quartz plate before entering the OPA. The time delay between pump and probe beams was carefully controlled by making the pump beam travel along a variable optical delay (ILS250, Newport). Intensities of the spectrally dispersed WLC probe pulses are monitored by a High Speed Spectrometer (Ultrafast Systems) for both visible and near-infrared measurements. To obtain the time-resolved transient absorption difference signal at a specific time, the pump pulses were chopped at 500 Hz and absorption spectra intensities were saved alternately with or without pump pulse. Typically, 4000 pulses excite the samples to obtain the fs-TA spectra at each delay time. The polarization angle between pump and probe beam was set at the magic angle (54.7°) using a Glan-laser polarizer with a half-wave retarder in order to prevent polarization-dependent signals. Cross-correlation fwhm in pump-probe experiments was less than 200 fs and chirp of WLC probe pulses was measured to be 800 fs in the 400-800 nm region. To minimize chirp, all reflection optics in the probe beam path and a quartz cell of 2 mm path length were used. After fs-TA experiments, the absorption spectra of all compounds were carefully examined to detect if there were any changes due to degradation and photo-oxidation of samples.

2. NMR spectra

NMR spectra of **2**: ^{1}H NMR (600.17 MHz, $CDCl_3$, 25 °C): δ = 8.68 (s, 1H; outer β-H), 8.67 (s, 1H; outer β-H), 8.47 (s, 1H; outer β-H), 8.16 (s, 1H; outer β-H), 7.96 (s, 1H; outer β-H), 7.88 (s, 1H; outer β-H), 7.12 (s, 1H; outer β-H), 6.79 (s, 1H; outer β-H), 6.03 (d, J = 4.6 Hz, 1H; boundary β-H), 5.88 (s, 1H; boundary β-H), 3.84 (s, 1H; boundary β-H), 3.47 (d, J = 5.5 Hz, 1H; boundary β-H), –0.19 (s, 1H; inner β-H), –0.35 (s, 1H; inner β-H), –0.43 (s, 1H; inner β-H), –1.22 (s, 1H; inner β-H) ppm; ^{19}F NMR (564.73 MHz, $CDCl_3$, 25 °C): –133.73 (m, 1F; *ortho*-F), –135.03 (d, J = 13.0 Hz, 1F; *ortho*-F), –135.26 (d, J = 13.0 Hz, 1F; *ortho*-F), –135.71 (d, J = 13.0 Hz, 1F; *ortho*-F), –136.46 (d, J = 13.0 Hz, 1F; *ortho*-F), –136.66 (d, J = 13.0 Hz, 1F; *ortho*-F), –137.28 (d, J = 13.0 Hz, 2F; *ortho*-F), –137.85 (m, 2F; *ortho*-F), –138.81 (d, J = 13.0 Hz, 1F; *ortho*-F), –139.25 (d, J = 26.0 Hz, 1F; *ortho*-F), –139.91 (d, J = 13.0 Hz, 1F; *ortho*-F), –140.35 (d, J = 9.1 Hz, 1F; *ortho*-F), –142.64 (d, J = 13.0 Hz, 1F; *ortho*-F), –144.45 (d, J = 13.0 Hz, 1F; *ortho*-F), –151.09 (t, J = 13.0 Hz, 1F; *para*-F), –153.74 (t, J = 13.0 Hz, 1F; *para*-F), –153.90 (t, J = 13.0 Hz, 1F; *para*-F), –154.17 (t, J = 13.0 Hz, 1F; *para*-F), –154.37 (t, J = 13.0 Hz, 1F; *para*-F), –155.89 (t, J = 13.0 Hz, 1F; *para*-F), –156.66 (t, J = 13.0 Hz, 1F; *para*-F), –157.93 (t, J = 13.0 Hz, 1F; *para*-F), –161 21 (s, 1F; *meta*-F), –161.87 (t, J = 13.0 Hz, 1F; *meta*-F), –162.03 (t, J = 13.0 Hz, 1F; *meta*-F), –162.21 (t, J = 13.0 Hz, 1F; *meta*-F), –162.64 (t, J = 13.0 Hz, 1F; *meta*-F), –164.02 (m, 2F; *meta*-F), –164.40 (m, 2F; *meta*-F), –164.77 (t, J = 13.0 Hz, 1F; *meta*-F), 164.98 (s, 1F; *meta*-F), –165.17 (s, 1F; *meta*-F), –165.60 (s, 2F; *meta*-F), –166.11 (s, 1F; *meta*-F), –168.60 (m, 1F; *meta*-F) ppm.

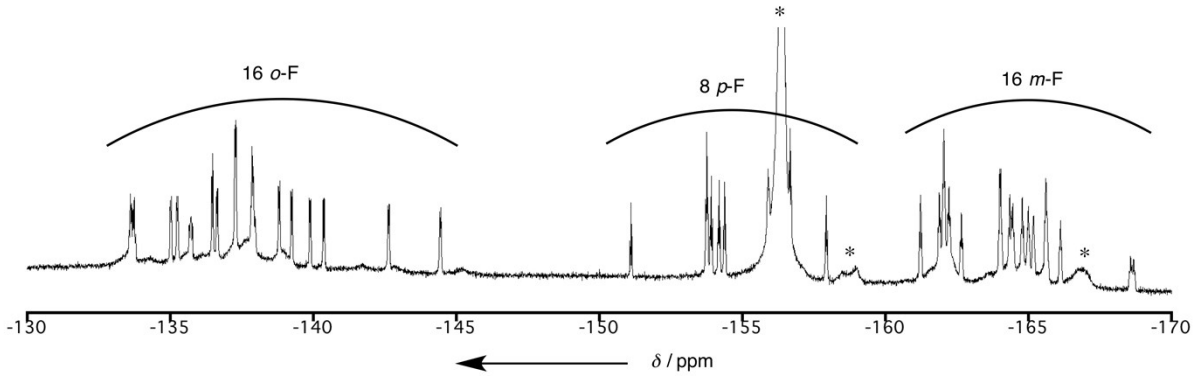

Fig. S1. ^{19}F NMR spectrum of **2** in $CDCl_3$ at 25 °C. Peaks marked with * are due to impurities. The sample was prepared by adding 40 equivalent of TBAF to a 4 mM solution of **1** in $CDCl_3$.

3. X-Ray Crystal Structure

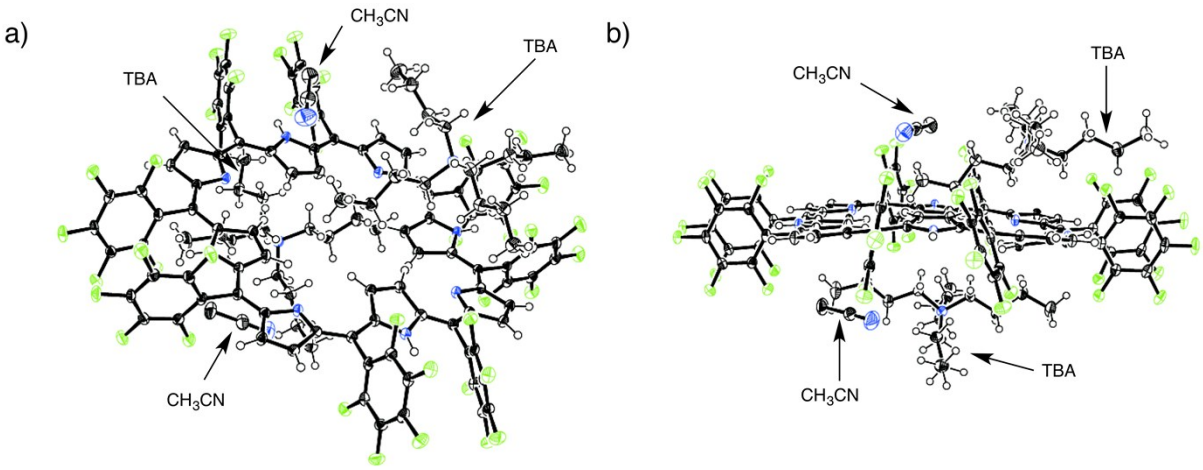

Fig. S2. X-Ray crystal structure of **3**. a) Top view and b) side view. The thermal ellipsoids are represented at 50% probabilities.

4. DFT Calculations

All calculations were carried out using the *Gaussian 09* program.[S1] Counter cations were omitted in **3**. All structures were fully optimized without any symmetry restriction. The calculations were performed by the density functional theory (DFT) method with restricted B3LYP (Becke's three-parameter hybrid exchange functionals and the Lee-Yang-Parr correlation functional) level,[S2,S3] employing a basis set 6-31G(d) for C, H, N, and F. The NICS values and absolute ^{1}H shielding values were obtained with the GIAO method at the B3LYP/6-31G(d) level. The global ring centers for the NICS values were designated at the nonweighted means of the carbon and nitrogen coordinates on the peripheral positions of macrocycles. In addition, NICS values were also calculated on centers of other local cyclic structures as depicted in the following figures.[S4] The ACID contours with vectors were obtained continuous set of gauge transformation (CSGT) methods[S5] at the same computational level for optimization processed based on optimized geometries without any modification.

a)

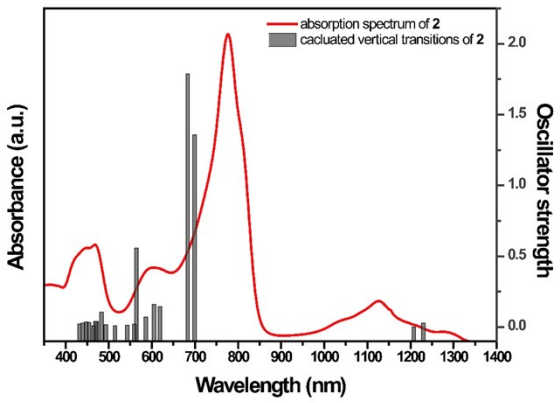

b)

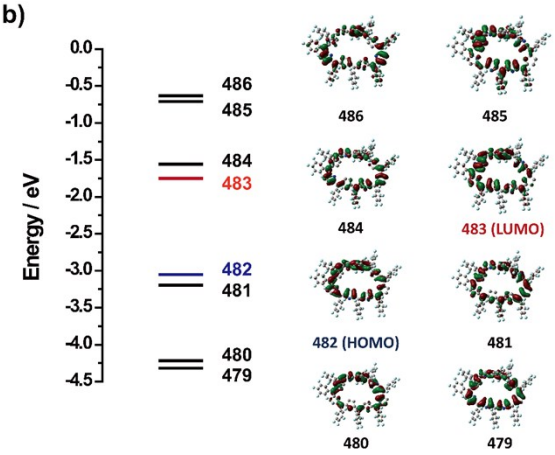

c)

Wavelength (nm)	Osc. Strength	Major Transitions
1230	0.0275	H → L (59%), H-1 → L+1 (41%)
1208	0.0009	H-1 → L (53%), H → L+1 (47%)
699	1.3576	H-1 → L+1 (32%), H → L (22%)
683	1.7891	H → L+1 (26%), H-1 → L (23%)

Fig. S3. a) Steady-state absorption spectrum and calculated vertical transitions, b) energy level diagrams and molecular orbitals, and c) major vertical transitions of **2**.

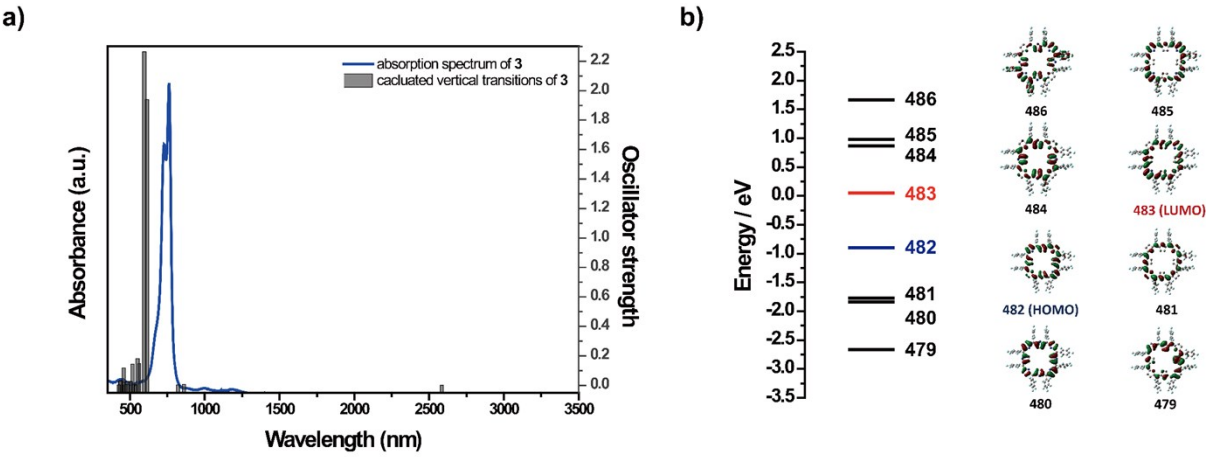

c)

Wavelength (nm)	Osc. Strength	Major Transitions
2585	0.0002	H → L (100%)
861	0.0069	H → L+1 (44%), H-1 → L (56%)
821	0.0017	H → L+2 (52%), H-2 → L (48%)
612	1.9403	H-1 → L (41%), H → L+3 (32%)
596	2.2649	H → L+3 (40%), H-2 → L (35%)
561	0.1472	H → L+3 (52%), H-1 → L (30%)
551	0.1823	H-1 → L+1 (54%), H-2 → L+2 (23%)

Fig. S4. a) Steady-state absorption spectrum and calculated vertical transitions, b) energy level diagrams and molecular orbitals, and c) major vertical transitions of **3**.

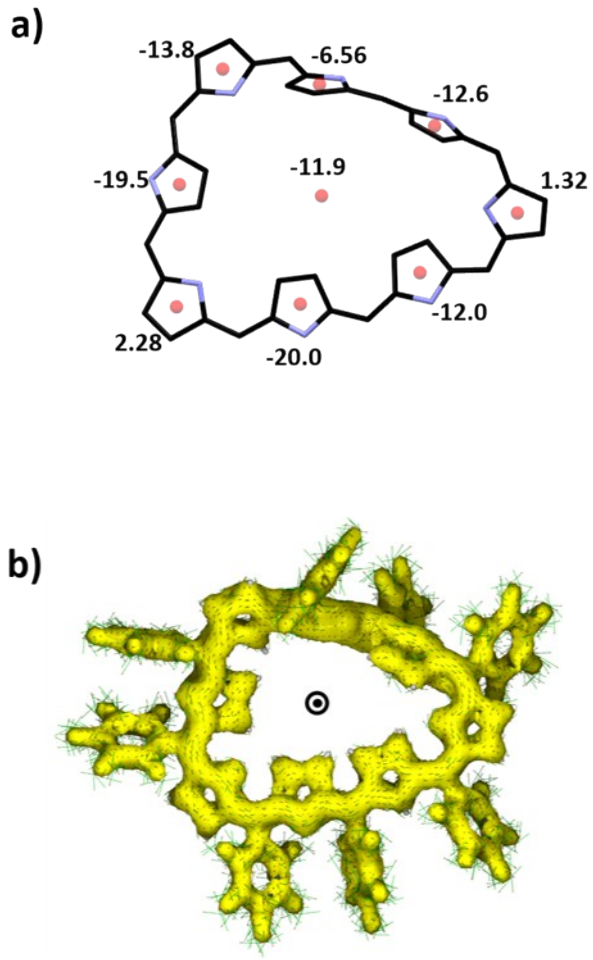

Fig. S5. a) NICS values of Bq ghost atoms for **2**. b) ACID plot of **2** at an isosurface value of 0.05. The external magnetic field is applied orthogonal to the molecule plane with vector point towards the viewer.

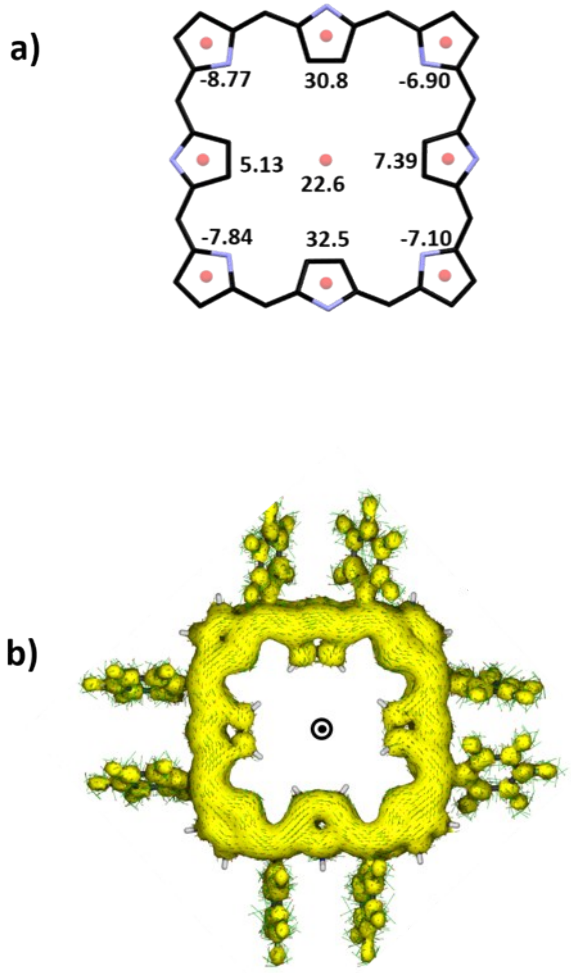

Fig. S6. a) NICS values of Bq ghost atoms for **3**. b) ACID plot of **3** at an isosurface value of 0.05. The external magnetic field is applied orthogonal to the molecule plane with vector point towards the viewer.

5. References

S1 Gaussian 09, Revision A.02, M. J. Frisch, G. W. Trucks, H. B. Schlegel, G. E. Scuseria, M. A. Robb, J. R. Cheeseman, G. Scalmani, V. Barone, B. Mennucci, G. A. Petersson, H. Nakatsuji, M. Caricato, X. Li, H. P. Hratchian, A. F. Izmaylov, J. Bloino, G. Zheng, J. L. Sonnenberg, M. Hada, M. Ehara, K. Toyota, R. Fukuda, J. Hasegawa, M. Ishida, T. Nakajima, Y. Honda, O. Kitao, H. Nakai, T. Vreven, J. A. Montgomery, Jr., J. E. Peralta, F. Ogliaro, M. Bearpark, J. J. Heyd, E. Brothers, K. N. Kudin, V. N. Staroverov, R. Kobayashi, J. Normand, K. Raghavachari, A. Rendell, J. C. Burant, S. S. Iyengar, J. Tomasi, M. Cossi, N. Rega, J. M. Millam, M. Klene, J. E. Knox, J. B. Cross, V. Bakken, C. Adamo, J. Jaramillo, R. Gomperts, R. E. Stratmann, O. Yazyev, A. J. Austin, R. Cammi, C. Pomelli, J. W. Ochterski, R. L. Martin, K. Morokuma, V. G. Zakrzewski, G. A. Voth, P. Salvador, J. J. Dannenberg, S. Dapprich, A. D. Daniels, O. Farkas, J. B. Foresman, J. V. Ortiz, J. Cioslowski, and D. J. Fox, Gaussian, Inc., Wallingford CT, 2009.

S2 A. D. Becke, *J. Chem. Phys.*, 1993, **98**, 1372.

S3 C. Lee, W. Yang and R. G. Parr, *Phys. Rev. B*, 1998, **37**, 785.

S4 (a) P. v. R. Schleyer, C. Maerker, A. Dransfeld, H. Jiao and N. J. R. v. E. Hommes, *J. Am. Chem. Soc*., 1996, **118**, 6317; (b) Z. Chen, C. S. Wannere, C. Corminboeuf, R. T. Puchta and P. v. R. Schleyer, *Chem. Rev*., 2005, **105**, 3842.

S5 T. A. Keith and R. F. W. Bader, *Chem. Phys. Lett*., 1993, **210**, 223.